

Chromospheric signatures of small-scale flux emergence as observed with NST and *Hinode* instruments

V. B. Yurchyshyn¹, P.R. Goode¹, V. I. Abramenko¹, J. Chae^{1,2}, W. Cao¹, A. Andic¹, K. Ahn¹

¹ *Big Bear Solar Observatory, New Jersey Institute of Technology, Big Bear City, CA 92314, USA*

² *Department of Physics and Astronomy, Seoul National University, Seoul 151-747, South Korea*

Received _____; accepted _____

ABSTRACT

With the ever increasing influx of high resolution images of the solar surface obtained at a multitude of wavelengths, various processes occurring at small spatial scales have become a greater focus of our attention. Complex small-scale magnetic fields have been reported that appear to have enough stored to heat the chromosphere. While significant progress has been made in understanding small-scale phenomena, many specifics remain elusive. We present here a detailed study of a single event of disappearance of a magnetic dipole and associated chromospheric activity. Based on New Solar Telescope $H\alpha$ data and *Hinode* photospheric line-of-sight magnetograms and Ca II H images we report the following. 1) Our analysis indicates that even very small dipoles (elements separated by about $0''.5$ or less) may reach the chromosphere and trigger non-negligible chromospheric activity. 2) Careful consideration of the magnetic environment where the new flux is deposited may shed light on the details of magnetic flux removal from the solar surface. We argue that the apparent collision and disappearance of two opposite polarity elements may not necessarily indicate their cancellation (i.e., reconnection, emergence of a “U” tube or submergence of Ω loops). In our case, the magnetic dipole disappeared by reconnecting with overlying large-scale inclined plage fields. 3) Bright points seen in off-band $H\alpha$ images are very well-correlated with the Ca II H bright points, which in turn are co-spatial with G-band bright points. We further speculate that, in general, $H\alpha$ bright points are expected to be co-spatial with photospheric BPs, however, a direct comparison is needed to refine their relationship.

1. Introduction

Fisher et al. (1998) showed that X-ray brightness of active regions is related to the intensity of photospheric magnetic fields. Abramenko et al. (2006) further elaborated that more complex and dynamic photospheric fields are usually associated with the brighter active regions (also see Brooks et al. (2008)). Although there is no general agreement as to what mechanisms are responsible for converting magnetic field energy into heat and transporting it toward the chromosphere and corona, a functional dependency between the magnetic field and coronal brightness was implemented in a number of models (Lundquist et al. 2004; Schrijver et al. 2004).

Only recently, have researchers come to recognize the importance of small-scale photospheric and chromospheric dynamics for heating and flare activity, e.g., Trujillo Bueno et al. (2004), proposed that the magnetic energy stored in the quiet photosphere is sufficient to heat the chromosphere. It was also suggested that a significant part of the heating is generated in the chromosphere in association with the occurrence of chromospheric jets, which are thought to be a manifestation of magnetic reconnection or dynamical waves (Shibata et al. 2007; ?). Recent *Hinode* data show that the photospheric fields are quite dynamic and complex even on very small scales (Centeno et al. 2007; Lites et al. 2007; Orozco Surez et al. 2008). Brooks et al. (2008) argues that heating mechanisms of transient events may be substantially different from that responsible for bright coronal loops, however they both may be related to highly dynamic magnetic fields. Abramenko et al. (2009) analyzed magnetic structures in mostly unipolar magnetic settings, such as coronal holes and plage regions, and concluded that the dynamics of energy release is associated with small spatial scales, on which magnetic field organization is quite entirely different. At this moment, there is no generally accepted mechanism to efficiently convert and transport quiet Sun magnetic energy into the corona. One of the big problems related to this issue is whether these small-scale fields (of order of 1'' or smaller) are at all capable of rising high enough to reach the chromosphere and thus transfer their stored energy. While some simulations show

that emerging Ω -type loops can reach the chromosphere, other model data indicate that these loops disintegrate at lower heights (Stein & Nordlund 2006). A statistical study of 69 flux emergence events (Martnez Gonzlez & Bellot Rubio 2009) concluded that only about 23% of the emerging dipoles can reach the chromosphere. Attempts to identify $H\alpha$ arch filament systems or other signatures associated with the emerging loops have been unsuccessful.

In this case study, we focus on a single event of small-scale magnetic flux cancellation and associated chromospheric activity. We will show that in mostly unipolar regions, associated with large-scale fields, even very small loops can rise high enough to transfer their energy into the chromosphere and corona.

2. Observations and Data Processing

New Solar Telescope (NST) in Big Bear Solar Observatory (BBSO) has a 1.7 m aspheric primary mirror with a 1.6 m clear aperture (Goode et al. 2010a,b). NST data used here were obtained at the telescope's Nasmyth focus with a 0.25\AA Zeiss Lyot birefringent $H\alpha$ filter cycling between $H\alpha-1.0\text{\AA}$ and $H\alpha+1.0\text{\AA}$. These off-band blue (red) shifted images make most apparent upward (downward) directed flows that have velocities up to 50 km/sec (seen as dark features in the respective images). The pixel size of the images is $0''.072$ and the field of view (FOV) is $67''\times 67''$. The original data were speckle reconstructed employing the KISIP speckle reconstruction code (Wger & von der Lhe 2007). Each reconstructed image was derived from 30 best images selected from a burst of 100 18 ms exposure images acquired in quick succession. It is generally recommended to use at least 70 images to successfully perform speckle reconstruction. However, we found that in cases of moderate seeing image selection improves contrast of the resulting image. The disadvantage of this approach is that the high frequency noise may increase, although it is not a concern for this study. The cadence of the reconstructed images is 8 sec. The resulting speckle reconstructed images were carefully aligned and destretched.

Hinode SOT (Kosugi et al. 2007; Tsuneta et al. 2008; Suematsu et al. 2008) data utilized here consist of line-of-sight magnetograms and Ca II H images. The narrowband filter imager (NFI) operated in a partial resolution mode with a pixel size of $0''.16$, FOV of $225'' \times 112''$ and the magnetic field data were collected on the Na I 5896\AA spectral line with a 3 minute cadence. The data have been processed with the standard SolarSoft package. The data numbers were then corrected for polarization sensitivity of the SOT instrumentation as described in Ichimoto et al. (2008). The resulting polarization signal was converted to magnetic flux density adopting weak field approximation as $B (Mx cm^{-2}) = \alpha * V/I$. Generally, α can be determined in several ways, ranging from a simple LTE calculation of Stokes-V response to the presence of the magnetic field to exploiting an empirical approach and comparing magnetograms from various instruments. Since there does not exist any standard calibration routine for *Hinode*/NFI magnetograms, we compared simultaneously recorded SOT/NFI V/I image and SOT/SP Level2 line of sight magnetic flux and varied parameter α to produce the most reasonable, in our view, agreement between the two magnetograms. For this comparison, we used the fraction of the magnetogram's FOV that contained only plage fields, thus excluding strong sunspot and pore fields. We found that applying $\alpha=10000$ under-estimates the resulting Na I 5896\AA total magnetic flux by about 10 times. When $\alpha=23000$ the total fluxes calculated from both magnetograms are equal, which, however, is hardly acceptable, since we expect the total magnetic field to weaken with height (Abramenko et al. 1992; Leka & Metcalf 2003) due to both expansion of the magnetic fields and the presence of short magnetic loops which close below the Na I 5896\AA line formation level. We therefore, chose parameter α based on the following: 1) the chromospheric/photospheric flux ratio should be about 0.50, and 2) the magnitude of the photospheric fields should be greater than that of the chromospheric fields by about 200–500 G (Abramenko et al. 1992; Leka & Metcalf 2003). We thus found that $\alpha =16000$ best satisfies the above requirements and this value was accepted as a calibration parameter. This parameter is two times higher than that used by Guglielmino et al. (2008), therefore, we realize that the produced magnetograms might represent

somewhat over-estimated magnitudes of the magnetic flux, which, however, is not critical for our study. Variations of α will introduce only insignificant changes in the total flux of magnetic elements and the flux change rates.

The Ca II H data came from the *Hinode*'s broadband filter imager, which operates with a pixel size of $0''.11$ and a FOV of $190'' \times 113''$. The NST and *Hinode* Ca II H images were carefully co-aligned by using bright points as a reference to an accuracy of better than $0''.25$. The correspondence between $H\alpha$ and Ca II H bright points is discussed in detail in next Section.

Data analyzed in this study were for active region (AR) NOAA 11048 acquired on 2010 February 17. NST observations span from 18:57UT until 20:10UT and overlap with *Hinode*'s coverage of this AR. STEREO data revealed that this slowly evolving active region first appeared on the solar disk at N23W45 on 2010 January 27.

3. Results

Figure 1 shows NST $H\alpha-1.0\text{\AA}$ (left) and $H\alpha$ line center (right) images taken at 19:44:04 UT and 19:44:12UT, respectively. The NST FOV covered only a very small fraction of the trailing part of the AR dominated by negative polarity fields. The box in Figure 1 encloses the area of interest shown in detail in Figure 2. The two upper panels in Figure 2 show a $22'' \times 22''$ portion of the AR plage, as seen in a $H\alpha-1.0\text{\AA}$ image taken at 19:47:34UT (background). This image was carefully co-aligned with a 19:47:35UT *Hinode*/SOT/FG magnetogram (contours, left) and a *Hinode* Ca II H image acquired at 19:47:32UT (contours, right). Magnetic field contours refer to ± 50 G and ± 150 G with red contours representing negative polarity. The lower left panel shows the same Ca II H image over-plotted with contours of the magnetic field. The lower right panel shows $H\alpha+1.0\text{\AA}$ image taken at 19:47:49UT over-plotted with the 19:47:35UT magnetogram.

The associated chromospheric activity appears to be typical for a plage region of a quiet

AR. There are numerous short lived dark striations associated with a network area seen against the photospheric background. These striations seem to be closely associated with the presence of bright points and, according to Rouppe van der Voort et al. (2009), they are rapid blue-shift events thought to be disk counterparts of type II spicules (De Pontieu et al. 2007).

The only active dynamic feature seen during the time interval was a dark recurrent jet-like feature rooted just outside a small pore, PR1. This feature could be identified at the beginning of the NST observations, however, its intensity was low. At about 19:30UT, the feature became active and its visibility in $H\alpha-1.0\text{\AA}$ peaked at about 19:47UT. At this moment, it was entirely absent in the red-shifted images, while its area and intensity in the center-line image was much weaker than that in the blue-shifted image. More precisely, some parts of the feature, mainly the tip of the jet, are not detectable in the $H\alpha$ center image, while the root of the jet appears dark at the line center, too). We therefore speculate that the tip of the jet-like may be associated with the spectral line shift (i.e., mostly plasma up-flows) while its root may display line asymmetry reflecting a broad spectra of plasma motions. In any case, the fact that the feature is seen in the far blue wing of the $H\alpha$ spectral line indicates that at least fraction of the plasma maybe moving at speeds up to 50km/s, which allows us to identify this feature as a chromospheric jet or $H\alpha$ surge. Numerous studies of surges (e.g., Chae et al. 1999; Yoshimura et al. 2003; Archontis et al. 2010) seem to agree that they are result of magnetic flux cancellation associated with new flux emergence. Taking into account that the magnetic field, associated with this jet, could be strongly inclined (as suggested by the presence of dark striations and their well-organized orientations), we may further speculate that the real velocity of the plasma motion could be even higher.

3.1. Comparison of Hinode Ca H II and NST H α images

H α -1.0 \AA images of the lower chromosphere reveal numerous bright points (BPs) forming long chains and/or small clusters. NST H α -1.25 \AA quiet Sun data (see Fig. 3 in Goode et al. (2010b)) also showed single BPs located at vertices of inter-granular lanes. These H α bright points (HBPs) could be related to the photospheric G-band bright points (GBPs), however, their exact association is not clear. The present data set does not include G-band images, however Berger & Title (2001) compared BPs detected with broadband G-band (4305 \AA) and Ca II K (3933 \AA) filters and a narrowband H α filter (6563 \AA). They concluded that large-scale patterns formed by GBPs and magnetic fields are well-correlated with the GBPs always having underlying magnetic fields (inverse is not true). Also, co-temporal H α -0.7 \AA images show increased intensity at the location of the GBPs, however, their correlation is weaker mainly because H α bright points are masked by numerous dark absorption features seen in the blue wing of the H α line. Otsuji et al. (2007) reported an association between the G-band and Ca II H bright points (CBPs) with the CBPs being larger. We, therefore, accept Ca II H bright points as a proxy for GBPs and address the issue of relationship between the H α bright points and concentrations of photospheric magnetic fields.

Figure 2 (upper right) shows an H α -1 \AA image over-plotted with contours of Ca II H radiation. Yellow contours indicate areas of enhanced brightening and dark red contours outline weak Ca II H emission associated with pores and the jet. The contour levels were set relatively high to avoid crowding the picture, so some weak CBPs are not plotted. As is evident from these panels, enhanced brightness in both spectral lines occurs at the locations of strong magnetic fields (see also Guglielmino et al. 2008). Also, areas of compact Ca II H brightenings are co-spatial with enhanced intensity at H α -1.0 \AA . Some HBPs may be at least partially due to enhanced heating caused by the interaction of magnetic elements in the photosphere. Because Ca II H and G-band BPs are also well correlated, we may further speculate that in general, H α -1.0 \AA BPs

are expected to be co-spatial with the GBPs, although a detailed analysis would be beneficial for better understanding of the lower chromosphere of the Sun.

3.2. Jet Related Dynamics

As is evident from Figure 2, the H α jet seems to be rooted in an area dominated by mixed polarity fields, and surrounded by mainly uni-polar, negative polarity plage-type fields. Figure 3 shows the evolution of these mixed polarity fields as seen in a series of *Hinode*/SOT/FG magnetograms spanning nearly one hour. New mixed polarity flux was constantly appearing in the upper half of the magnetogram. Here we will focus on only one instance of new flux emergence. Visual inspection of the sequence of the magnetograms revealed that at about 19:14UT a small, elongated negative polarity magnetic ridge, N1, began moving toward the center of the image (direction of the displacement is indicated by the arrow). Estimates yield the average speed of the ridge to be about 1.5 km s^{-1} , which is a typical speed of granular flows (Kubo et al. 2010). As the displacement progressed, a positive polarity element, P1, began to appear on the right side of the ridge as if the moving ridge was piling up pre-existing positive fields in front of it. The closest distance between P1 and N1 centers of gravity measured at 19:50UT was about 0.5 Mm. The two magnetograms taken before 19:47UT clearly show weak positive fields “scattered” in front of the ridge, so that merging (coalescence) of magnetic fields was indeed possible. Another possibility is that a new magnetic dipole emerged at this location. Even though there is no solid evidence to support the merging of a pre-existing flux, this possibility, in general, cannot be excluded and a non-negligible fraction of newly appearing dipoles may have this character. Should it be confirmed when it is statistically studied, the merging nature of new flux appearance may affect our current understanding of flux transport and visible appearance of through the solar surface.

As it follows from the magnetograms (Figure 3), the positive magnetic flux confined to P1

began to decrease after 19:49UT and it completely disappeared from the box in Figure 3 by 20:05UT, while the remnants of N1 seemed to migrate to the top of the box and eventually left the area. Along with P1, the positive polarity immediately to the south-west of P1 (lower right corner of the box) disappeared too. Although P1 and N1 show all the signs of canceling magnetic features, such as converging motion with subsequent disappearance, we argue that the line of separation between P1 and N1 may not be a site of magnetic cancellation, rather, P1 and N1 comprised one magnetic dipole.

Figure 4 shows the evolution of the magnetic flux enclosed in the box in Figure 3. Positive polarity flux (solid line) was steadily increasing and it peaked at about 19:49UT, with the maximum flux density being about 200 G. The negative polarity flux (dashed) does not show any changes consistent with positive flux variations, mainly because the corresponding negative flux changes would be only about 7% of the pre-existing flux (6.0×10^{18} Mx) and barely discernible in the plot. After 19:49UT, the positive flux began to decrease and fell by 4.0×10^{17} Mx over a period of 11 min, which implies that the magnetic flux changed at a rate of 6.1×10^{14} Mx s⁻¹ (we will call it the cancellation rate). Chae et al. (2002) defined a specific cancellation rate, which is the cancellation rate divided by the length of the cancellation interface. If we take the interface to be equal to 0.5 Mm (full width of P1) the specific cancellation rate is then 1.3×10^7 Mx s⁻¹ cm⁻¹, which is very similar to the rate of 8×10^6 Mx s⁻¹ cm⁻¹ reported in Park et al. (2009).

Nearly simultaneously with the enhancement of P1, the dark jet becomes active and very distinct in blue-shifted H α images (Figure 3, middle row), while the co-temporal Ca II H data (Figure 3, bottom row) acquired with a broadband filter showed only weak signs of the jet. Although not visible in the gray-scale image (Figure 2, lower left), the Ca II H jet can be distinguished in the contour plot (Figure 2, upper right), where the blue contours are co-spatial with the H α -1.0Å jet. Two bright patches, (BP1 and BP2) nearly co-spatial with P1 and P2 and seen

in off-band $H\alpha$ at 19:47UT, as well as Ca II H images, similarly revived with enhancement of P1. After 19:50UT they appeared in the Ca II H images to be connected by bright diffuse structures, which could be interpreted as magnetic loops connecting magnetic elements P2-N1. Note that Guglielmino et al. (2008) in Figure 3 show similar loop like structures connecting a dipole. After 19:50UT the bright patch, BP2, associated with P2 and N2 suddenly brightened and began to rapidly change shape. The shape and brightness evolution corresponded to that observed during formation and cooling of post-eruptive arcades, although insufficient spatial resolution precludes us from having solid evidence to support this claim. The red-shifted $H\alpha$ image over-plotted with magnetic field contours (Figure 2, lower right) clearly indicates the presence of a well-pronounced dark downflow patch centered at the P1 element. Red-shifted data taken at 20:00 UT also show a dark, high contrast loop connecting the pore PR1 and P1 fields. These relatively strong downflows could be related either to the plasma downdrafts along the newly formed loops (similar to downflows in post-eruption arcades) or to the submergence of these loops.

To interpret the above sequence of events and the dynamics of magnetic connection during this event, we start with Figure 5. Here we present two possible initial magnetic configurations and the results of their evolution. First, we assume that magnetic elements P1 and N1 are not connected and belong to different magnetic systems (Figure 5, left). Please, note that the discussed development is also applicable to the case when P1 and N1 are footpoints of an emerging “U”-type loop. The dotted lines represent magnetic connections before the event. As N1 approaches P1 they cancel each other via a reconnection event that should occur low in the chromosphere and photosphere. As a result, two new connections are formed (solid lines) and P1 and N1 are now connected by a short loop 2, which is expected to submerge, so that P1 and N1 disappear beneath the solar surface. While this scenario traditionally treats two approaching magnetic elements as canceling features, it seems to fail at reproducing the variety of observed features such as the large-scale jet, the bright Ca II H loops connecting N1 and P2, the $H\alpha$ - 1.0\AA loop connecting PR1 and P1, activity at N2 and disappearance of magnetic fields at PR1,

P2 and N2.

In the right panels of Figure 5, we present an alternative view of this event. Here we assume that the magnetic elements N1 and P1 comprise one dipole. Here, too, the dotted lines represent magnetic connections before the event. As N1 (the negative polarity ridge) moves towards P1 and enhances it (or as the P1-N1 dipole emerges), magnetic loop 2, connecting them, expands and eventually reconnects with the opposite directed large-scale fields 1. This interchange reconnection makes line 1 to “jump” over the dipole and a chromospheric jet will be associated with it (e.g., Isobe et al. 2008). At the same time, element P1 becomes connected to the large area of negative polarity field associated with pore PR1 (these connecting lines will later be visible in 20:00UT red-shifted images). As this first reconnection proceeds, newly created lines 4 will eventually similarly interact with the P2-N2 dipole, which would lead to another interchange reconnection and formation of a new connection between P2 and N1 (see diffuse structures connecting P2 and N1 in the lower left panel of Figure 2). This second reconnection begins at about 19:50UT, when a chromospheric patch brightens up between P2 and N1. As a result of this multi-step restructuring, a fraction of large-scale plage field lines will “migrate” away from the pore, while newly created dipoles P2-N1 and P1-PR1 will fully or partially cancel (submerge).

The latter possibility appears to be more successful in explaining the observed events. However, in this scenario no cancellation occurs between P1-N1 since it treats the two approaching magnetic elements as being pre-connected, which is not a commonly accepted interpretation, although it is quite plausible. This alternative approach may also explain why instruments fail to detect strong horizontal fields at many cancellation sites (Kubo et al. 2010).

4. Conclusions and Discussion

- 1) Our data and analysis show that even very small dipoles (distance between the elements of order of $0''.5$ or less) may reach the chromosphere and manifest themselves via non-negligible chromospheric activity.
- 2) Careful consideration of the magnetic environment where the new flux is deposited may shed light on the details of magnetic flux removal from the solar surface. We argue that the apparent collision and disappearance of two opposite polarity elements may not necessarily indicate their cancellation (i.e., reconnection, emergence of a “U” tube or submergence of Ω loops). In our case, the magnetic dipole disappeared by reconnecting with overlying large-scale inclined plage fields.
- 3) Bright points seen in the off-band $H\alpha$ images are very well-correlated with the Ca II H bright points, which in turn are co-spatial with G-band bright points. We further speculate that, in general, $H\alpha$ bright points expected be co-spatial with photospheric BPs, however, a direct comparison is needed to refine their relationship.

Small-scale magnetic fields and associated dynamics have recently come to the center of attention. It was discovered that magnetic flux emerges on very small scales and it is complex (Centeno et al. 2007; Lites et al. 2007; Orozco Surez et al. 2008; Abramenko et al. 2009). Trujillo Bueno et al. (2004) and ? claim that these small-scale fields may have enough stored energy to heat the chromosphere. Abramenko et al. (2009) reported that quiet Sun magnetic fields are highly intermittent and complex on scales below 2 Mm and they may determine the energy release dynamics needed for chromospheric heating. Shibata et al. (2007) observed Ca II H jets in active regions near the limb and argued that they are evidence of ubiquitous small-scale reconnection, which may be the source of the chromospheric and coronal heating. Goode et al. (2010b) recently discovered even tinier $H\alpha$ jet-like structures in an inter-network field. Thus, the interaction of the small-scale quiet Sun loops with large-scale fields may be a conduit for

transferring the stored energy up into the chromosphere and corona (Martnez Gonzlez et al. 2010). While some researchers connect chromospheric jets to reconnection between various magnetic structures, others argue that a large variety of chromospheric dynamics can be modeled with a wave-driven reconnection (?), i.e., small scale emerging fields may not be essential for chromospheric and coronal energy balance. Moreover, model calculations also seem to suggest (Stein & Nordlund 2006) that small-scale loops cannot reach chromospheric heights, thus deeming this transport mechanism as not plausible. Martnez Gonzlez & Bellot Rubio (2009) reported that about 77% of loops indeed never rise high enough (or, at least, they were not strong enough) to show up in chromospheric magnetograms. This case study shows that even smallest dipoles (0.5 Mm) may interact with the overlying large-scale fields and, provided that the magnetic environment is favorable (dipole and overlying fields are oppositely directed), have a significant effect in the chromosphere including re-structuring of the magnetic field as well as heating and plasma acceleration.

Another issue that our data enables us to address is the process of magnetic flux cancellation. It is accepted now that two magnetic elements of opposite polarity are canceling if they display converging motions and subsequently disappear from line-of-sight magnetograms. The current state of this research is still inconclusive: various studies report that canceling magnetic features may be associated with both emerging or submerging magnetic fields (see recent paper by Lida et al. (2010) for more discussion). The direction of the horizontal magnetic field between two canceling features may help resolve the issue, however, the 180 degree ambiguity does not allow us to draw any definitive conclusions. Observed vertical flows at the cancellation site are often used as an argument to support one view or another, however, these flows may often be associated with down-drafting plasma along, say, a stationary magnetic loop rather than with the submergence of an entire loop.

We propose that this problem can benefit from studies of the magnetic environment where

the cancellation occurs. Analysing magnetic connections before and after the cancellation may lead to more definite conclusions. We, therefore, argue that although the magnetic dipole in our study displayed properties of canceling features, it was not a canceling magnetic feature but rather newly appearing magnetic loops. The flux cancellation occurred as a result of penetration of the dipole's loops into the chromosphere and their follow-on interaction with large-scale fields. We also speculate that in this case, the newly appearing dipole could probably be due enhancement (merging) of an existing weak flux by converging granular flows, as opposed to an emergence of a new flux through the solar surface. Similar conclusions come from a statistical study by Lamb et al. (2008), who argue that a large fraction of magnetic flux observed in the quiet Sun could be due to the coalescence of previously existing weak and unresolved flux into concentrations that are large and strong enough to be detected. This is certainly a possibility that deserves further exploration.

We thank referee for careful reading of the manuscript and valuable suggestions and criticism that led to significant improvement of the paper. Hinode is a Japanese mission developed and launched by ISAS/JAXA, with NAOJ as domestic partner and NASA and STFC (UK) as international partners. It is operated by these agencies in co-operation with ESA and NSC (Norway). Authors thank BBSO observers and instrument team for their contribution into this study. VY work was supported under NASA's GI NNX08AJ20G and LWS TR&T NNG0-5GN34G grants. VA acknowledges support from NSF grant ATM-0716512.

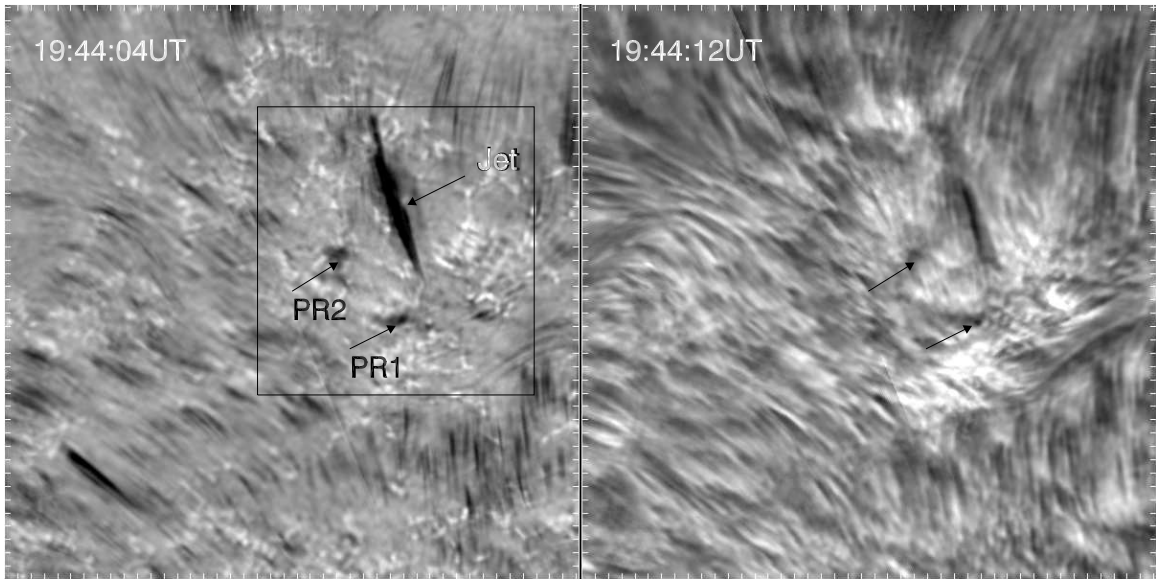


Fig. 1.— Chromospheric images of AR NOAA 11048 as seen with NST. Left panel is a 19:44:04UT off-band $H\alpha-1.0\text{\AA}$ image of the trailing part of the AR, while the right panel shows a nearly simultaneous $H\alpha$ line center image of the same area. Two arrows indicate two small pores and the box outlines the region of interest. The dark jet-like feature seen in the left panel appears barely discernible in the line center image, which indicates that nearly all associated plasma move toward the observer with speeds approaching 50km/s. The tick marks at the edge of the images indicate 1'' intervals.

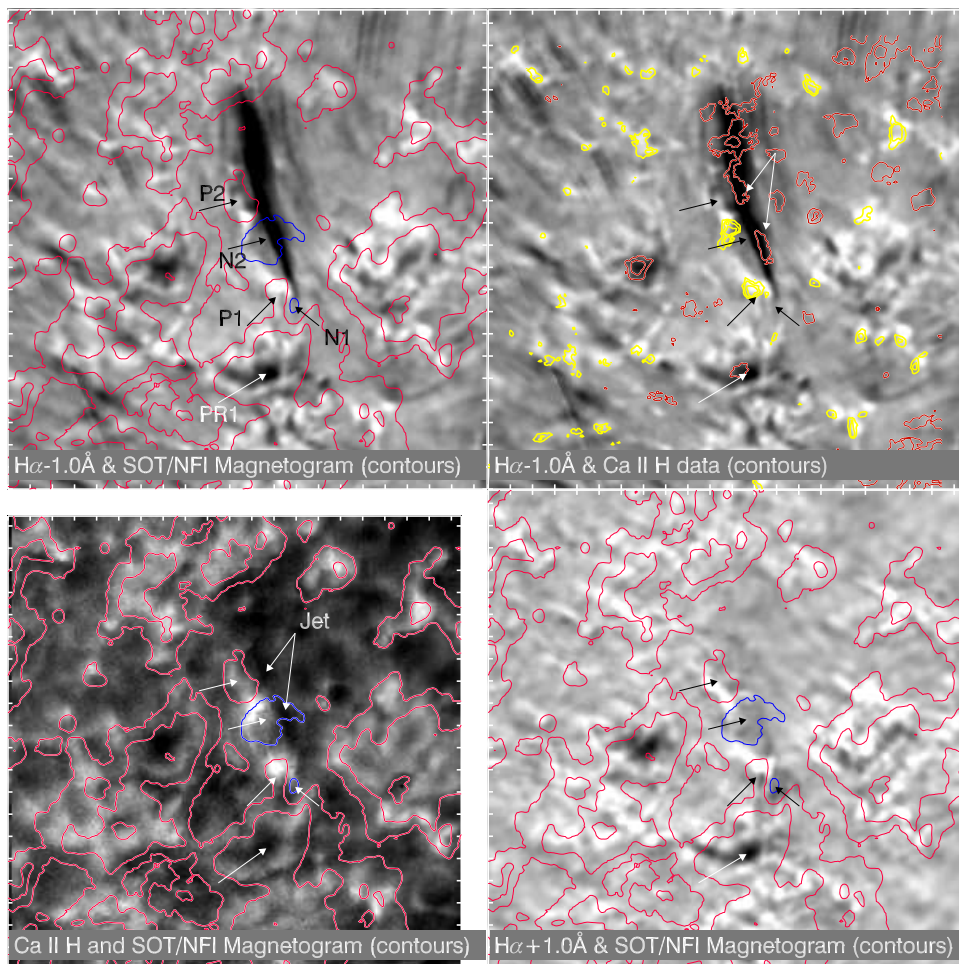


Fig. 2.— Chromospheric images of AR NOAA 11048 as observed with NST and *Hinode* instruments. The backgrounds in the top panels are the NST $H\alpha$ -1.0Å image (19:47:34UT) of Figure 1; in the lower left panel – *Hinode* Ca II H emission (19:47:32UT) and the lower right panel – NST $H\alpha$ +1.0Å image (19:47:49UT) of Figure 1. For comparison, the upper right image is overplotted with contours of 19:47:32UT *Hinode* Ca II H emission, while the other three images are overplotted with contours of the 19:47:35UT *Hinode*/FG magnetogram. The magnetic field contours are plotted at ± 50 and ± 150 G levels with red (blue) contours referring to negative (positive) magnetic polarity. The dark red (yellow) contours in the upper right panel refer to arbitrary levels chosen to best indicate darkest (brightest) parts of Ca II H emission without over-crowding the image. The tick marks at the edge of the images separate $1''$ intervals. Arrows indicate locations of various features discussed in the text.

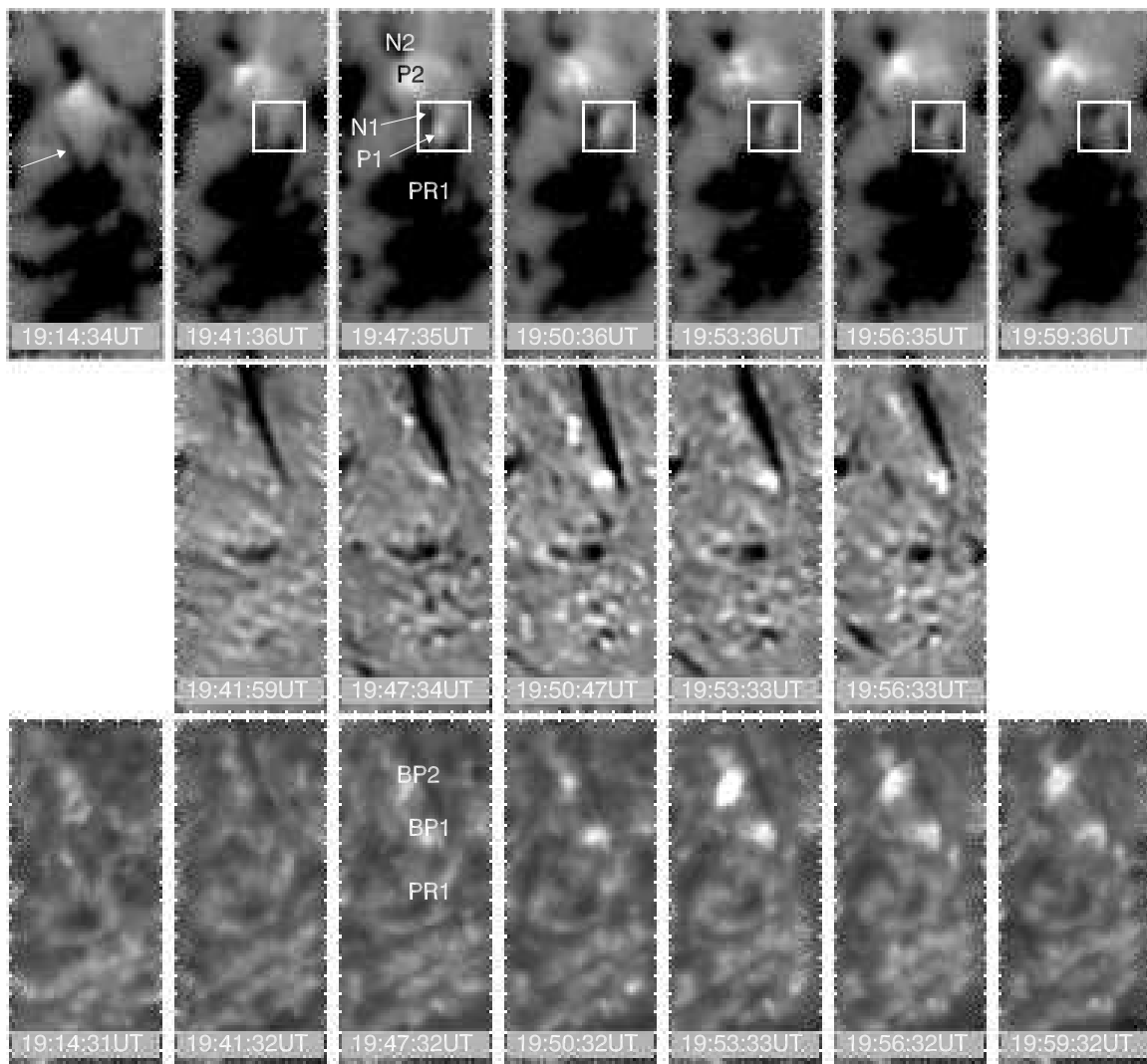


Fig. 3.— Evolution of the magnetic field surrounding the flux cancellation event as derived from *Hinode*/SOT/FG magnetograms (top), BBSO/NST $H\alpha$ -0.75Å (middle) and *Hinode* Ca II H (bottom) images. The data span is nearly one hour. New mixed polarity flux was constantly appearing in the area between the negative (dark) and positive (white) polarities. The arrow in the first top panel indicates the direction of the displacement of negative polarity element, N1. Location of a small pore is indicated with PR1. P1, N2 and P2 mark locations of magnetic elements discussed in the text. The box encloses the area used to measure variations of magnetic flux. The tick mark separation is 1".

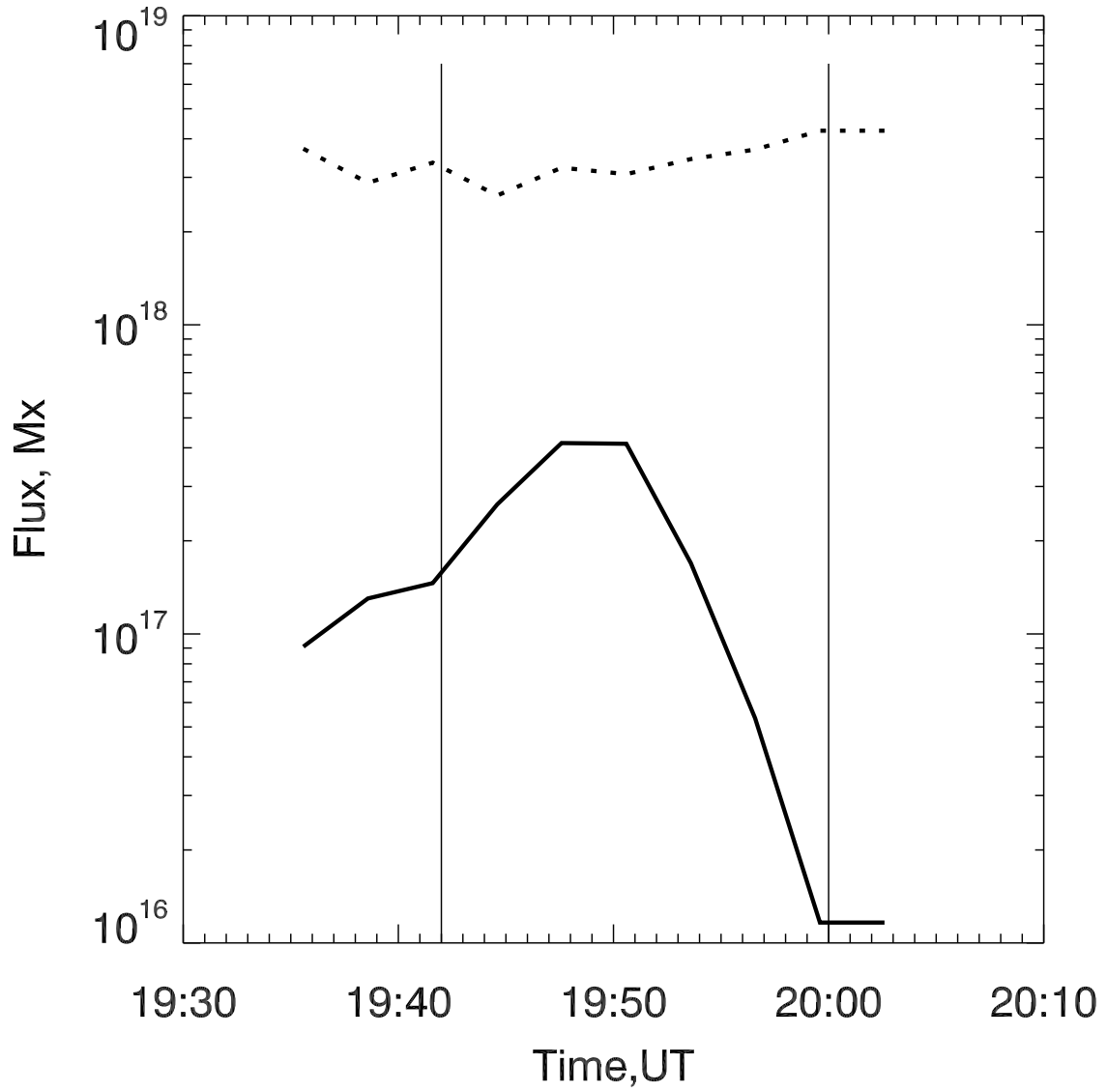


Fig. 4.— Time profiles of positive (solid) and negative (dashed) magnetic flux measured inside the box shown in Fig. 3. Between 19:50UT and 20:00UT, the positive magnetic flux decreased by 4.0×10^{17} Mx.

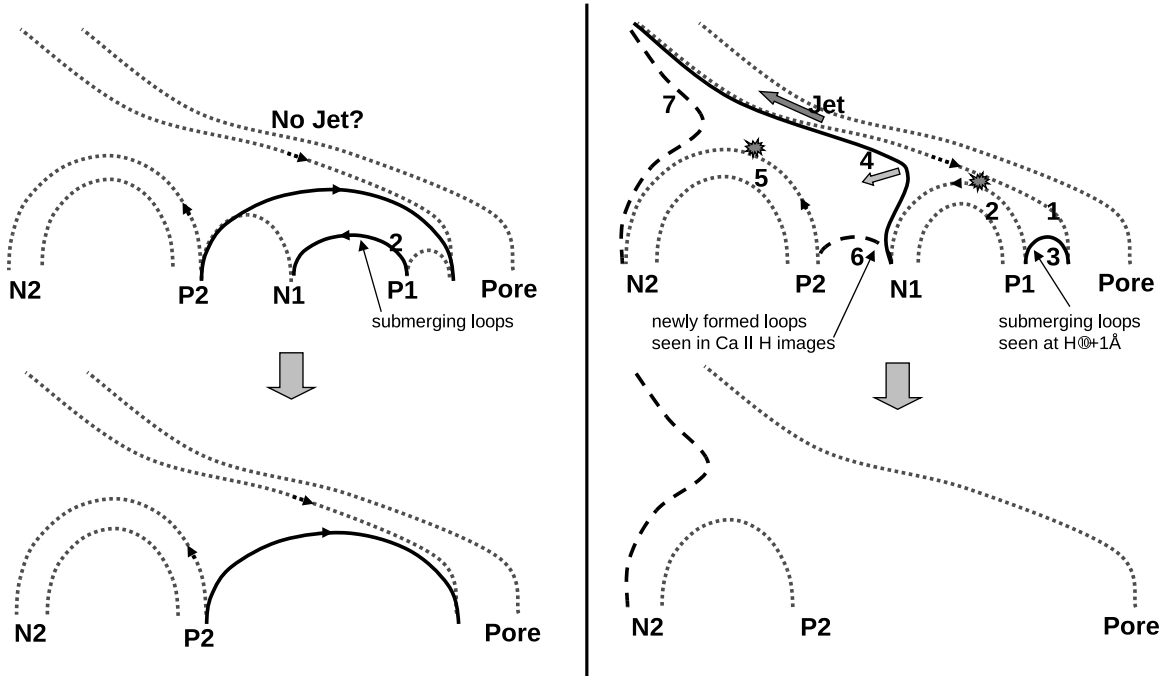


Fig. 5.— Possible scenarios of flux interaction and reconnection. In all panels the light gray dotted lines represent magnetic connection before the cancellation event. Bottom panels show resulting magnetic connections. Left: P1 and N1 are connected. Lines 3 and 4 represent magnetic connections formed during first reconnection event between 1 and 2. Lines 6 and 7 are formed due to the second reconnection event. Right: P1 and N1 belong to different magnetic systems. Submerging Line 2 is a results of cancellation between P1 and N1.

REFERENCES

- Abramenko, V., Gopasyuk, S. I., Ogir', M. B., & Yurchyshyn, V. 1992, *Kinematics and Physics of Celestial Bodies*, 8, 43
- Abramenko, V. I., Pevtsov, A. A., & Romano, P. 2006, *ApJ*, 646, L81
- Abramenko, V. I., Yurchyshyn, V., & Watanabe, H. 2009, *Sol. Phys.*, 260, 43
- Archontis, V., Tsinganos, K., & Gontikakis, C. 2010, *Astron. Astrophys.*, 512, L2
- Berger, T., & Title, A. M. 2001, *ApJ*, 553, 449
- Brooks, D. H., Ugarte-Urra, I., & Warren, H. P. 2008, *ApJ*, 689, L77
- Centeno, R., et al. 2007, *ApJ*, 666, L137
- Chae, J., Moon, Y., Wang, H., & Yun, H. S. 2002, *Sol. Phys.*, 207, 73
- Chae, J., Qiu, J., Wang, H., & Goode, P. R. 1999, *ApJ*, 513, L75
- De Pontieu, B., et al. 2007, *PASJ*, 59, 655
- Fisher, G. H., Longcope, D. W., Metcalf, T. R., & Pevtsov, A. A. 1998, *ApJ*, 508, 885
- Goode, P. R., Coulter, R., Gorceix, N., Yurchyshyn, V., & Cao, W. 2010a, *Astronomische Nachrichten*, 88, 789
- Goode, P. R., Yurchyshyn, V., Cao, W., Abramenko, V. I., Andic, A., Ahn, K., & Chae, J. 2010b, *ApJ*, 714, L31
- Guglielmino, S. L., Zuccarello, F., Romano, P., & Bellot Rubio, L. R. 2008, *ApJ*, 688, L111
- Ichimoto, K., et al. 2008, *Sol. Phys.*, 249, 233
- Iida, Y., Yokoyama, T., & Ichimoto, K. 2010, *ApJ*, 713, 325

Isobe, H., Proctor, M. R. E., & Weiss, N. O. 2008, *ApJ*, 679, L57

Kosugi, T., et al. 2007, *Sol. Phys.*, 243, 3

Kubo, M., Low, B. C., & Lites, B. 2010, *ApJ*, 712, 1321

Lamb, D. A., DeForest, C. E., Hagenaar, H. J., Parnell, C. E., & Welsch, B. T. 2008, *ApJ*, 674, 520

Leka, K. D., & Metcalf, T. R. 2003, *Sol. Phys.*, 212, 361

Lites, B., et al. 2007, *PASJ*, 59, 571

Lundquist, L. L., Fisher, G. H., McTiernan, J. M., & Rgnier, S. 2004, in *ESA Special Publication*, Vol. 575, *SOHO 15 Coronal Heating*, ed. R. W. Walsh, J. Ireland, D. Danesy, & B. Fleck, 306–30+

Martnez Gonzlez, M. J., & Bellot Rubio, L. R. 2009, *ApJ*, 700, 1391

Martnez Gonzlez, M. J., Manso Sainz, R., Asensio Ramos, A., & Bellot Rubio, L. R. 2010, *ApJ*, 714, L94

Orozco Surez, D., Bellot Rubio, L. R., del Toro Iniesta, J. C., & Tsuneta, S. 2008, *Astron. Astrophys.*, 481, L33

Otsuji, K., et al. 2007, *PASJ*, 59, 649

Park, S., Chae, J., & Litvinenko, Y. E. 2009, *ApJ*, 704, L71

Roupe van der Voort, L., Leenaarts, J., De Pontieu, B., Carlsson, M., & Vissers, G. 2009, *ApJ*, 705, 272

Schrijver, C. J., Sandman, A. W., Aschwanden, M. J., & De Rosa, M. L. 2004, *ApJ*, 615, 512

Shibata, K., et al. 2007, *Science*, 318, 1591

Stein, R. F., & Nordlund, . 2006, *ApJ*, 642, 1246

Suematsu, Y., et al. 2008, *Sol. Phys.*, 249, 197

Trujillo Bueno, J., Shchukina, N., & Asensio Ramos, A. 2004, *Nature*, 430, 326

Tsuneta, S., et al. 2008, *Sol. Phys.*, 249, 167

Wger, F., & von der Lhe, O. 2007, *Appl. Opt.*, 46, 8015

Yoshimura, K., Kurokawa, H., Shimojo, M., & Shine, R. 2003, *PASJ*, 55, 313